REPORT DOCUMENTATION PAGE

Form Approved OMB No. 074-0188

1. AGENCY USE ONLY (Leave blank)	2. REPORT DATE	3. REPORT TYPE AND DATES COVERED
	July 1997	SPIE Conference, 27 July – 1 August 1997

4. TITLE AND SUBTITLE
Diode-laser absorption sensor system for measurements of combustion pollutants

5. FUNDING NUMBERS
N/A

6. AUTHOR(S)
R.M. Mihalcea, D.S. Baer, R.K. Hanson

7. PERFORMING ORGANIZATION NAME(S) AND ADDRESS(ES)
High Temperature Gasdynamics Laboratory
Department of Mechanical Engineering
Stanford University
Stanford, CA 94305-3032

8. PERFORMING ORGANIZATION REPORT NUMBER
Paper Number: 3172 10

9. SPONSORING / MONITORING AGENCY NAME(S) AND ADDRESS(ES)
SERDP
901 North Stuart St. Suite 303
Arlington, VA 22203

10. SPONSORING / MONITORING AGENCY REPORT NUMBER
N/A

11. SUPPLEMENTARY NOTES

12a. DISTRIBUTION / AVAILABILITY STATEMENT
Approved for public release: distribution is unlimited

12b. DISTRIBUTION CODE
A

13. ABSTRACT *(Maximum 200 Words)*
A diode-laser sensor system has been applied to measure the concentrations of NO, N2O, CO, and CO2 in combustion gases using absorption spectroscopy and fast extraction-sampling techniques. Measured survey spectra of the NO 3v band (R branch) and H2O lines from the v2+v3 band in the spectral region from 5556 cm-1 to 5562 cm-1 were recorded and compared to calculated spectra to select optimum transitions for NO detection. Similarly, measured survey spectra of the N2O 3v3 band from 6535 cm-1 to 6600 cn-1 were used to identify optimum transitions for N2O detection. High resolution NO absorption measurements were recorded in a gast-flow multipass cell containing probe-sampled combustion gases to determine NO concentrations in a laminar, premixed CH4/air flame, seeded with NH3. For fuel-rich conditions, the fraction of NH3 converted to NO decreased with increasing equivalence ratio. In additional experiments, CO and CO2 absorption measurements were used to determine species concentrations above a laminar, premixed CH4/air flame. Good agreement was found between measured CO and CO2 concentrations and calculated chemical equilibrium values.

14. SUBJECT TERMS
diode laser; external-cavity diode laser; sensors; absorption spectroscopy; combustion pollutants; SERDP; SERDP Collection

15. NUMBER OF PAGES
12

16. PRICE CODE N/A

17. SECURITY CLASSIFICATION OF REPORT	18. SECURITY CLASSIFICATION OF THIS PAGE	19. SECURITY CLASSIFICATION OF ABSTRACT	20. LIMITATION OF ABSTRACT
unclass.	unclass.	unclass.	UL

NSN 7540-01-280-5500

Standard Form 298 (Rev. 2-89)
Prescribed by ANSI Std. Z39-18
298-102

SPIE Conference, 27 July – 1 August, 1997, San Diego, CA Paper Number: 3172 10

Diode-laser absorption sensor system for measurements of combustion pollutants

R. M. Mihalcea, D. S. Baer, and R. K. Hanson

High Temperature Gasdynamics Laboratory
Department of Mechanical Engineering
Stanford University, Stanford, CA 94305-3032

ABSTRACT

A diode-laser sensor system has been applied to measure the concentrations of NO, N_2O, CO, and CO_2 in combustion gases using absorption spectroscopy and fast extraction-sampling techniques. Measured survey spectra of the NO 3ν band (R branch) and H_2O lines from the $\nu_2+\nu_3$ band in the spectral region from 5556 cm^{-1} to 5572 cm^{-1} were recorded and compared to calculated spectra to select optimum transitions for NO detection. Similarly, measured survey spectra of the N_2O $3\nu_3$ band from 6535 cm^{-1} to 6600 cm^{-1} were used to identify optimum transitions for N_2O detection. High-resolution NO absorption measurements ($R_2(7.5)$ and $R_1(7.5)$ lines) were recorded in a fast-flow multipass cell containing probe-sampled combustion gases to determine NO concentrations in a laminar, premixed CH_4/air flame, seeded with NH_3. For fuel-lean conditions, the measured NO mole fractions corresponded to 68% of the injected NH_3. For fuel-rich conditions, the fraction of NH_3 converted to NO decreased with increasing equivalence ratio. In additional experiments, CO and CO_2 absorption measurements (R(13) line of the 3ν band and R(16) line of the $2\nu_1+2\nu_2^0+\nu_3$ band, respectively) were used to determine species concentrations above a laminar, premixed CH_4/air flame. Good agreement was found between measured CO and CO_2 concentrations and calculated chemical equilibrium values.

Keywords: diode laser, external-cavity diode laser, sensors, absorption spectroscopy, combustion pollutants

1. INTRODUCTION

Recent developments in semiconductor diode-laser technology have extended the range of available laser wavelengths and, hence, the number of accessible species that may be probed using absorption spectroscopy techniques. For example, room-temperature, narrow-linewidth tunable sources near 1.8 μm enable absolute concentration measurements of NO (3ν band), an important combustion-generated pollutant.[1] Near-IR lasers operating near 1.34 μm–1.39 μm (H_2O), 1.56 μm (CO), 1.57 μm (CO_2), and 1.65 μm (CH_4, C_2H_4, CH_3Cl) have been successfully applied to measure species concentrations in a variety of environments.[2-5] Additionally, near-UV and visible diode lasers near 0.39 μm (frequency doubled) and 0.67 μm (NO_2), and 0.76 μm (O_2) enhance the variety of accessible species and, thus, the range of possible applications.[6,7]

NO and CO are toxic substances and major combustion-generated pollutants that are facing increasingly strict emission regulations. Global increases in N_2O and CO_2 levels have been attributed to antrophogenic sources, in particular to increased combustion of biomass and fossil fuels. N_2O and CO_2 contribute to the greenhouse effect and are currently being discussed as candidates for future emission regulations.[8] A diode-laser sensor system, capable of measuring these species, might be incorporated in combustion-control applications to reduce pollutant emissions and increase fuel efficiency.

Further author information –
R. M. Mihalcea (correspondence): Email: radu@navier.stanford.edu; Telephone: (415) 725-2024; Fax: (415) 723-1748
D. S. Baer: Email: dsb@navier.stanford.edu; Telephone: (415) 725-4016
R. K. Hanson: Email: hanson@navier.stanford.edu; Telephone: (415) 723-1745

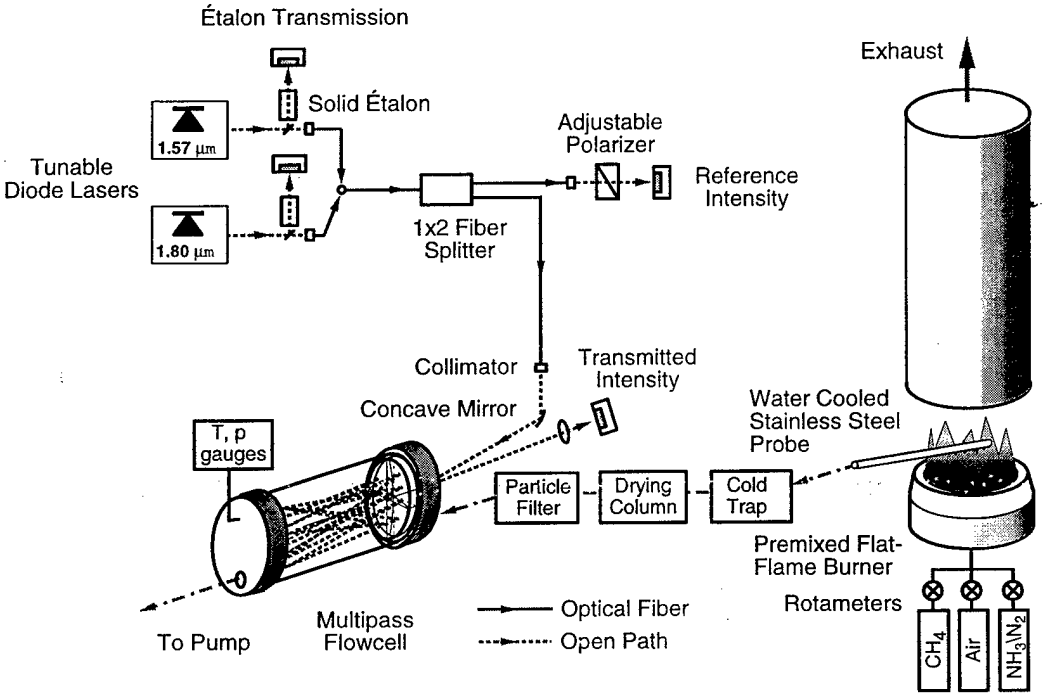

Fig. 1 Schematic diagram of the diode-laser sensor system experiment used to measure NO, N_2O, CO, and CO_2 mole fractions in sampled combustion gases.

The aim of the present work is to develop a fiber-optic diode-laser system to measure NO, N_2O, CO, and CO_2 in combustion environments using absorption spectroscopy and fast-extraction sampling techniques. Initial experiments served to improve the spectroscopic database and to determine the optimum transitions for species detection. An on-line data reduction system was developed to convert measured absorption spectra automatically into species mole fraction values using the previously obtained spectroscopic parameters.

Measured NO survey spectra (3v band, R branch) in the spectral region from 5556–5572 cm^{-1} were recorded in a multipass cell and compared with calculated values using published spectroscopic parameters and an existing expression for the electric dipole moment of the $X^2\Pi$ ground state of NO. Additional measurements of H_2O in the same spectral region were performed to select optimum NO lines with maximum detectivity and minimum H_2O interference. Measured N_2O survey spectra in the spectral region from 6535–6600 cm^{-1} were recorded and compared to calculated H_2O survey spectra to identify optimum transitions for N_2O measurements.

In the first set of sampling experiments, the diode laser absorption sensor system was applied to measure NO molefractions in a premixed CH_4/air flame, seeded with NH_3. In the second set of measurements, the system was used to measure CO and CO_2 concentrations in combustion gases from a non-seeded, premixed CH_4/air flame.

2. EXPERIMENTAL DETAILS AND THEORY

Figure 1 is a schematic of the experimental setup consisting of the burner, the fast-sampling apparatus, and the diode-laser system. A water-cooled, premixed, flat-flame burner (McKenna) with a 6-cm diameter served as the combustion test facility. Methane, air, and 30% NH_3/N_2 flows were metered with calibrated rotameters, premixed, and injected into the burner. The 30% NH_3 in N_2 mixture was supplied at flow rates of 0.24 l/min and 0.43 l/min. For the typical operating conditions (3.0 l/min CH_4 and 19.5–42.4 l/min air, no NH_3/N_2 injection), the stoichiometry was varied between equivalence ratios of ϕ= 0.67 to 1.47.

Post-flame gas temperatures were measured with uncoated type-S thermocouples (3 mil wire diameter) and corrected for radiation losses. The measurement location was 2 cm above the burner and 1.5 cm from the sampling probe where no probe-induced combustion-gas cooling was observable. The estimated uncertainty in the measured temperatures, ± 20 K, was primarily due to uncertainty in bead size.

A water-cooled stainless steel probe (4.1-mm internal diameter) with four inlet holes of 0.50-mm diameter was used to continuously sample (choked flow) combustion gases 2 cm above the burner. The samples were drawn through an ice-bath-cooled water trap, a drying column, and a two-stage filter to reduce the water mole fraction and to remove particles. Temperature and static pressure in the absorption cell were monitored using a type-S thermocouple and an MKS Baratron pressure gauge with a full scale range of 1 atm and accuracy of ±1%. The cell temperature remained within 1 K above ambient levels during all measurements, confirming that the sampled gas had been effectively cooled. The sampled flow entered the cell on the same end as the optical beam and exited on the opposite end through 1/2-inch diameter ports before being drawn through a two-stage rotary pump and vented into the exhaust stack.

The diode-laser system consisted of a distributed feedback (DFB) InGaAsP diode laser operating between 5556 cm^{-1} and 5572 cm^{-1} (case temperature between 50 and 5°C) and an external cavity InGaAsP diode laser (ECDL) with a spectral tuning range between 6321–6680 cm^{-1}. Individual lineshape measurements with the DFB laser were recorded over a 0.8 cm^{-1}–1.0 cm^{-1} spectral window by varying the injection current using a sawtooth waveform at 1.25 Hz. H_2O survey spectra between 5556 cm^{-1} and 5572 cm^{-1} were measured by temperature tuning the DFB laser. N_2O survey spectra were recorded with the ECDL by using the internal wavelength ramp function of the ECDL controller. Measurements of individual transitions of CO, CO_2, and N_2O (1.0-cm^{-1} scans) were made by adjusting the internal grating of the ECDL to the respective center wavelengths and by applying a 6-volt sawtooth voltage waveform at a 1.25-Hz repetition rate to the wavelength modulation input. A Burleigh wavemeter was used for absolute wavelength measurements.

Each laser output was passed through an optical isolator to prevent reflections into the laser cavity and split into two beams using 30-min wedged beam splitters. The reflected beams were directed through solid étalons, with free spectral ranges of 2.0 GHz, to monitor the wavelength tuning of the laser. The transmitted beams were focused into optical fibers (8-μm core diameter) and guided to a 1×2 fiber splitter. One output from the splitter was used to measure the reference intensity, I_o. The other output was directed into the multipass absorption cell and focused at the exit onto a detector to measure the transmitted intensity, I. Germanium and InGaAs detectors (300 kHz bandwidth (-3dB)) were used to measure signals near 1.8 μm and 1.5 μm, respectively.

The multipass cell (0.3-liter-volume) consisted of two astigmatic mirrors (20-cm separation) that allowed for a high absorption path to volume ratio, ideal for fast-flow applications. In sampling experiments, the pumping speed was approximately 0.4 l/s and the resulting cell response time (0 to 90% of the final value) was ~1s.[4] The effective absorption path was determined from absorption measurements of CH_4 and O_2 and known line strengths for various cell pressures between 0–760 torr. The measured effective absorption path was 3276 cm. The estimated pathlength uncertainty (2%) was primarily due to uncertainty in linestrength. The total measurement uncertainty of individual transitions probed was estimated to be ~4% owing to mixture fraction uncertainty (2%), pathlength uncertainty (2%), uncertainty in pressure measurements (1%), and uncertainty in the computed area under each Voigt profile (1%).

An on-line data analysis system (Figure 2) was developed for the sampling experiments to calculate species mole fractions from the measured transmission, reference, and étalon signals. A 200-MHz Pentium MMX personal computer served as a computational platform using LabVIEW® as the graphical programming language. Transmission and reference signals, I and I_o, were analog low-pass filtered (200-Hz passband) to avoid aliasing and subtracted to cancel common mode noise. The difference, reference, and étalon signals, were then digitized using a 12-bit A/D converter and transferred to the computer. Additional digital signal processing (FIR filter, 20-Hz passband) further reduced noise without introducing phase distortion. For typical operating conditions, signal-to-noise levels of ~40 dB were achieved. The étalon signal was used to convert the difference and reference signals from the time domain into the optical frequency domain.

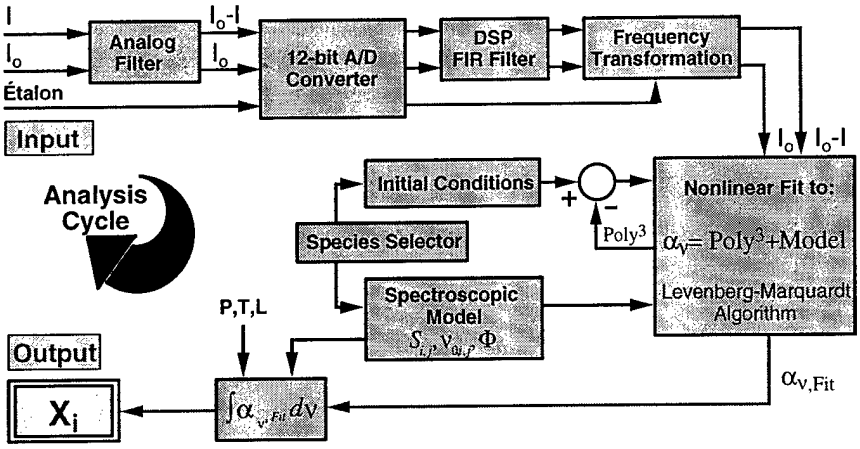

Fig. 2 Schematic diagram of the on-line data analysis system to determine species concentrations from measured absorption spectra.

The spectral absorbance α_ν is related to measured difference and reference signals, I_o-I and I_o, via Beer-Lambert's relation

$$\alpha_\nu = -\ln\left(1-\frac{I_o - I}{I_o}\right). \tag{1}$$

The spectral absorbance is linearly dependent on the mole fraction X_i of species i with M_i overlapping absorption lines by

$$\alpha_\nu = PX_iL\sum_{j=1}^{M_i} S_{i,j}(T)\Phi_{i,j}(\nu - \nu_{0,i,j}, a_{i,j}), \tag{2}$$

where P is the total pressure (atm), L is the absorption pathlength (cm), $S_{i,j}$ is the temperature-dependent linestrength of line j and species i (cm^{-2}/atm), and Φ is the lineshape function (cm). Mole fractions of species i, X_i, were determined by iteratively fitting the measured absorbance to a previously established spectroscopic model containing relative line positions and linestrengths, and to a third-order polynomial that accounted for the unbalanced response between the reference and the transmission detector. The least-squares fitting procedure incorporated the nonlinear Levenberg-Marquardt algorithm and converged within two iterations to best-fit multi-line Voigt profiles. Integration of the fitted Voigt profiles over a 2 cm^{-1} spectral window and application of Equation (2) yielded reliable mole fraction values.

3. RESULTS

3.1 Spectroscopic Studies

The lack of spectroscopic data for the NO 3v band (not included in HITRAN96) and the need to predict line positions and intensities for the selection of appropriate laser wavelengths motivated the fundamental spectroscopic computations.

The coupling of rotation and electronic motion of the NO $X^2\Pi$ ground state represents an intermediate case between Hund's case (a) and (b) with transition from case (a) to (b) with increasing nuclear rotation.[9] For the J″ of interest, Hund's case (a) was a good approximation and the selection rules were chosen accordingly. As a result, the $^2\Pi \leftarrow ^2\Pi$ band splits into two sub-bands, $^2\Pi_{1/2} \leftarrow ^2\Pi_{1/2}$ and $^2\Pi_{3/2} \leftarrow ^2\Pi_{3/2}$, corresponding to an F_2 and an F_1 manifold, respectively. The energy

levels for the $X^2\Pi$ ground state of NO were calculated, neglecting Λ-type doubling, by numerical diagonalization of the Hamiltonian matrix using published matrix elements.[10] Einstein A coefficients were calculated using

$$A_{(v',J',\Omega-v'',J'',\Omega'')} = \frac{64\pi^4 \nu^3}{3hc^3} |R|^2 q_{v'v''} \frac{S_R}{2J'+1}, \tag{3}$$

where R is the transition moment integral, $q_{v'v''}$ is the Franck-Condon factor, and S_R is the Hönl-London factor. The transition moment integral was calculated on the basis of a rotationless transition by

$$R = \langle v' | \mu(r) | v'' \rangle, \tag{4}$$

for v′=3 and v″=0 using an existing expression for the electronic dipole moment μ(r) and previously published spectroscopic constants.[10-12]

Figure 3 shows the calculated absorption spectra for the NO 3ν band (1 atm and 296 K). A universal broadening coefficient of $2\gamma = 0.13$ cm^{-1}/atm was used to model the collisional contribution to the linewidth. The spectra exhibits a P-Q-R structure with a weak Q-branch. The strongest transitions occur in the R branch in the spectral region between 5562 cm^{-1} and 5580 cm^{-1} with approximately 60% higher values than the strongest P branch transitions.

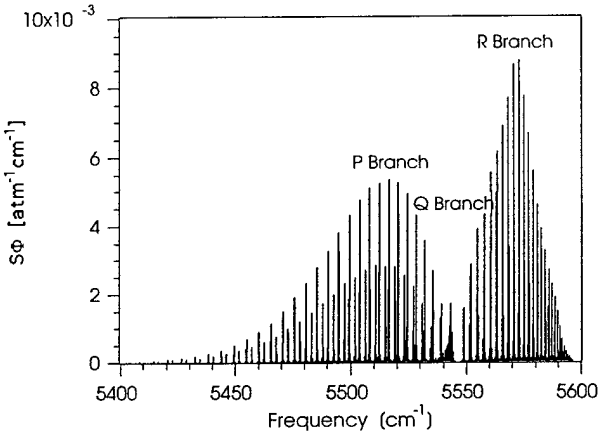

Fig. 3 Calculated absorption spectra of the NO 3ν band for 296 K and 1 atm. A universal broadening coefficient of $2\gamma = 0.13$ cm^{-1}/atm was used to model the collisional contribution to each individual linewidth.

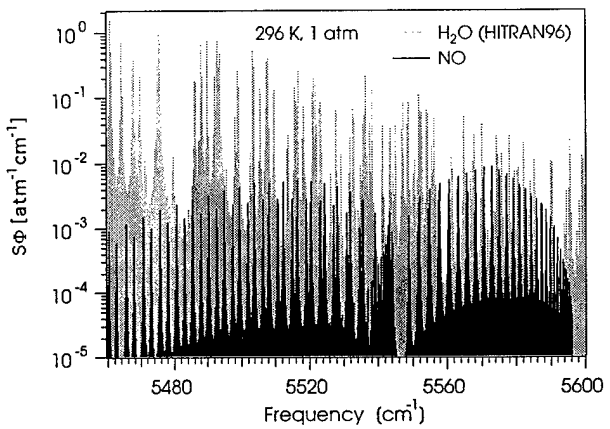

Fig. 4 Comparison of the calculated NO (3ν band) and H_2O spectra in the spectral region between 5460 cm^{-1}–5600 cm^{-1} (296 K, 1 atm).

In addition to identifying strong transitions it is important to analyze interfering absorption from other species for the successful selection of laser wavelengths. In room air, the major interference arises from H_2O absorption. Figure 4 compares the calculated NO and H_2O spectra (using the HITRAN96 database) for conditions of 296 K and 1 atm. H_2O lines are more than 40 times stronger than NO transitions (5460–5550 cm^{-1}) and decrease in intensity with increasing frequency. The spectral region between 5556 cm^{-1} and 5578 cm^{-1} (R branch of NO) seems most promising since it contains strong NO transitions and relatively weak and sparse H_2O lines.

Figure 5 is a plot of the measured NO survey spectra within the DFB laser tuning range (5556–5572 cm^{-1}) obtained at 296 K, 240 torr, and 5020 ppm NO in N_2. The spectra were constructed by recording several 0.8–1.0 cm^{-1} interval scans. The $^2\Pi_{1/2} \leftarrow {}^2\Pi_{1/2}$ and $^2\Pi_{3/2} \leftarrow {}^2\Pi_{3/2}$ subbands are clearly distinguishable for J″<8.5.

Figure 6 is a plot of the measured Λ-doubled line pairs $R_{2e}(7.5)+R_{2f}(7.5)$ and $R_{1e}(7.5)+R_{1f}(7.5)$ (296 K, 240 torr, 5020 ppm NO in N_2). Contributions from the $^2\Pi_{3/2}\leftarrow{}^2\Pi_{3/2}$ and $^2\Pi_{3/2}\leftarrow{}^2\Pi_{3/2}$ subbands are illustrated as broken lines. The residual corresponds to the normalized difference between the data and the 2-line best-fit Voigt profile. Λ-type doubling was not resolved since its magnitude was approximately one order of magnitude lower than the Doppler contribution to the linewidth ($\Delta\nu_D = 1.25\times10^{-2}$ cm^{-1} at 296 K and 5568.3 cm^{-1}).[13] A comparison of the measured and calculated line positions and intensities of the $R_{2e}(7.5)+R_{2f}(7.5)$ and $R_{1e}(7.5)+R_{1f}(7.5)$ line pairs is shown in Table 1. Good agreement was found between calculated and measured line intensities.

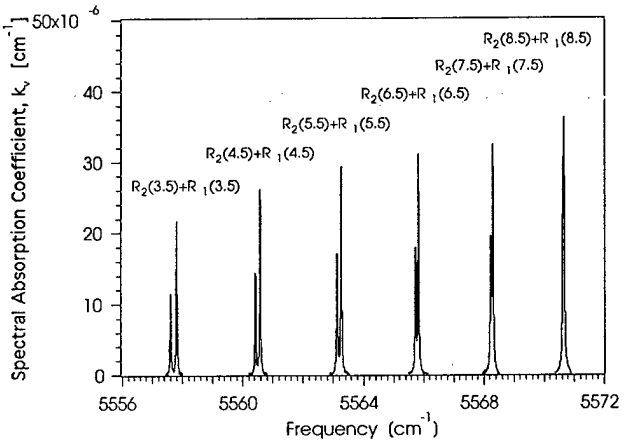

Fig. 5 Measured NO survey spectra (3ν band, R branch) between 5556 cm^{-1} and 5572 cm^{-1} (296 K, 240 torr, 5020 ppm NO in N_2).

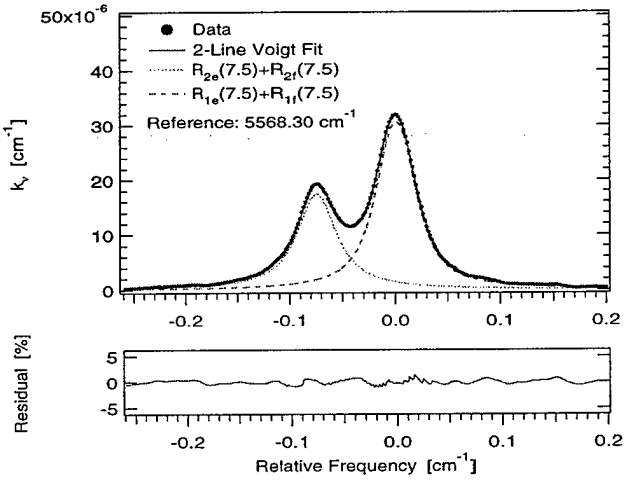

Fig. 6 Single-sweep measurement of the spectral absorption coefficient obtained by tuning the DFB laser over the Λ-doubled line pairs $R_{2e}(7.5)+R_{2f}(7.5)$ and $R_{1e}(7.5)+R_{1f}(7.5)$ of NO near 5568.3 cm^{-1} (296 K, 240 torr, 5020 ppm NO in N_2).

	Line Position			**Line Strength (296 K)**		
Transition	measured [cm^{-1}]	calculated [cm^{-1}]	difference meas.-calc. [cm^{-1}]	measured [cm^{-2}/atm]	calculated [cm^{-2}/atm]	diff. rel. to calculated [%]
$R_{2e}(7.5)+R_{2f}(7.5)$	5568.23	5568.25	-0.02	6.91×10^{-4}	6.81×10^{-4}	1.5
$R_{1e}(7.5)+R_{1f}(7.5)$	5568.30	5568.32	-0.02	1.19×10^{-3}	1.27×10^{-3}	-6.0

Table 1 Comparison of measured and calculated line positions and line strengths of the $R_{2e}(7.5)+R_{2f}(7.5)$ and $R_{1e}(7.5)+R_{1f}(7.5)$ Λ-doubled line pairs at 296 K.

Figure 7 shows a) the measured and b) the calculated (HITRAN96) spectral absorption coefficient of H_2O between 5556–5571 cm^{-1} (297 K, 114 torr, 1.15% H_2O in air). All measured strong lines are also predicted by HITRAN96. Measured peak heights are (on average) 10% lower than calculated values. Measured line strengths, however, are within ±7% of HITRAN96 values, suggesting that broadening coefficients may be inaccurate. Measured line positions generally agree with the HITRAN96 database to within the wavemeter reading accuracy of ±0.01 cm^{-1}.

Figure 8 shows the comparison of a) measured and b) calculated (HITRAN96) spectral features of H_2O in a 0.2 cm^{-1} spectral window near 5567.75 cm^{-1} (297 K, 114 torr, 1.15% H_2O in air). The measurements indicate that the actual spectral separation between the overlapping lineshapes is 0.02 cm^{-1} and not 0.011 cm^{-1} as listed in HITRAN96. The measured sum linestrength of both features is within 1% of the tabulated value in the HITRAN96 database.

A comparison of measured NO and H_2O survey spectra showed that most NO lines in the region between 5556–5572 cm^{-1} are free of H_2O spectral interference. For maximum detectivity and minimum H_2O interference, the $R_{2e}(7.5)+R_{2f}(7.5)$ and $R_{1e}(7.5)+R_{1f}(7.5)$ Λ-doubled line pair was chosen to determine NO mole fractions in sampling experiments.

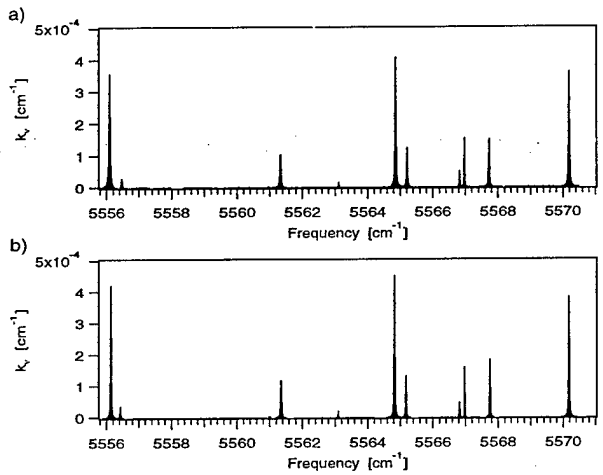

Fig. 7 Comparison of the a) measured and b) calculated (HITRAN96) spectral absorption coefficient of H_2O between 5556 cm^{-1} and 5571 cm^{-1} for cell conditions of 297 K, 114 torr, 1.15% H_2O in air.

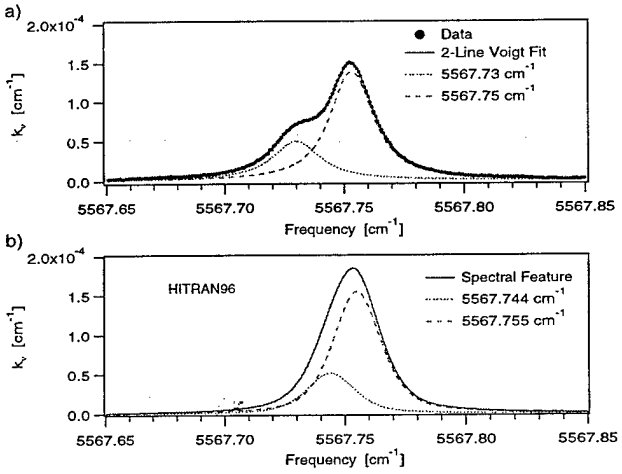

Fig. 8 Comparison of the a) measured and b) calculated (HITRAN96) spectral absorption coefficient of H_2O in a 0.2 cm^{-1} spectral window near 5567.75 cm^{-1} (297 K, 114 torr, 1.15% H_2O in air).

Although N_2O has been studied in the near-IR using Fourier transform spectroscopy, no line strength data are available.[14] Figure 9 shows the measured survey spectra of the N_2O $3\nu_3$ band and line assignments in the spectral range from 6535

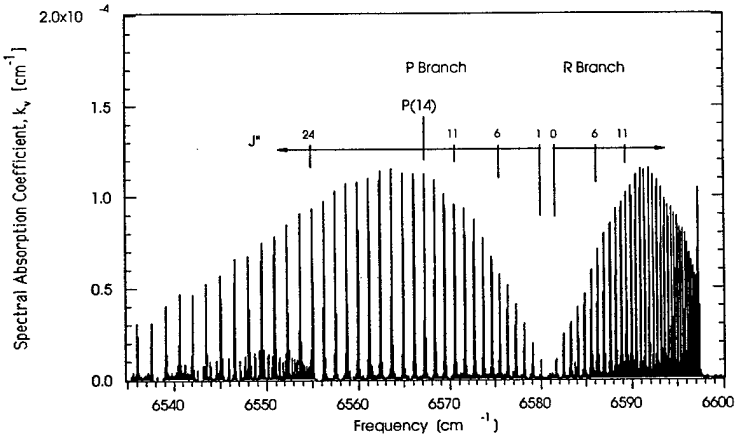

Fig. 9 Measured survey spectra of the N_2O $3\nu_3$ band in the spectral range from 6535–6600 cm^{-1} (297 K, 272 torr, 5.0% N_2O in air). Indicated is the P(14) line that was used for sampling experiments.

cm^{-1}–6600 cm^{-1} (297 K, 272 torr, 5.0% N_2O in air). Comparison of the measured N_2O survey spectra with calculated H_2O spectra (HITRAN96) were performed to select optimum transitions for N_2O measurements. The indicated P(14) transition was well isolatedfrom spectral H_2O interference ($\nu_1+2\nu_2$ and $2\nu_2+\nu_3$ bands) and was chosen for N_2O detection. Line position and line strength values are listed in Table 2.

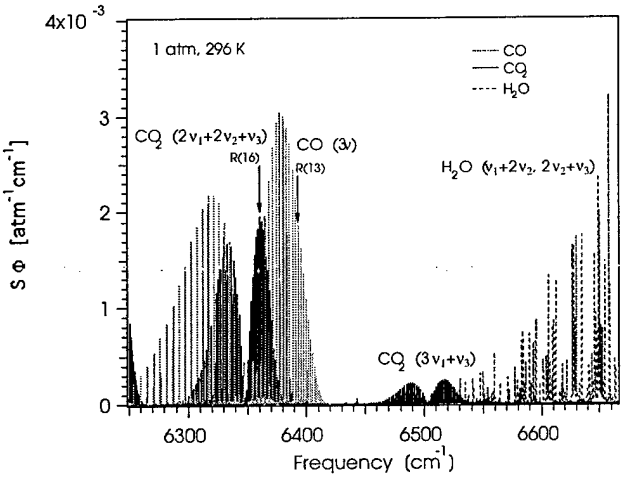

Fig. 10 Calculated survey spectra (HITRAN96) of CO, CO_2, and H_2O in the spectral range from 6250 cm^{-1} to 6666 cm^{-1} for 296 K and 1 atm. Indicated are the R(13) line of the CO 3ν band and the R(16) line of the CO_2 $2\nu_1+2\nu_2^0+\nu_3$ band that were used to determine species mole fractions.

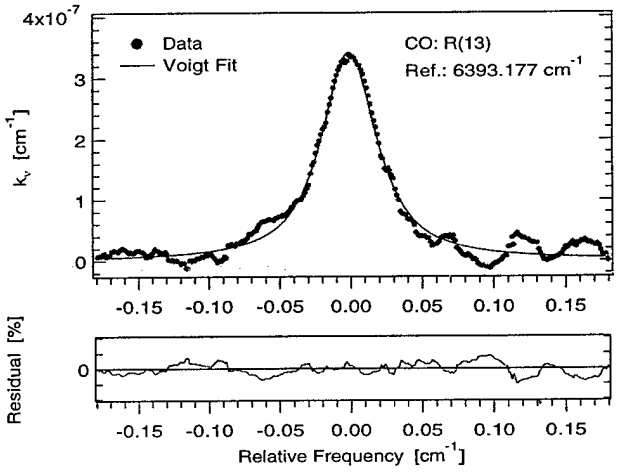

Fig. 11 Single-sweep measurement of the R(13) line of CO (296 K, 214 torr, 230-ppm CO). The residual represents the normalized difference between the best-fit Voigt profile and the data.

Figure 10 is a plot of the calculated survey spectra (HITRAN96) of CO, CO_2, and H_2O in the spectral range from 6250 cm^{-1} to 6666 cm^{-1} for 296 K and 1 atm. Indicated are the R(13) line of the CO 3ν band and the R(16) line of the CO_2 $2\nu_1+2\nu_2^0+\nu_3$ band that were used to determine species specific mole fractions. These lines were chosen to avoid mutual interference between CO and CO_2 absorption and to maximize species detectivity. Measured survey spectra and linestrengths of CO, CO_2, and H_2O have been published previously.[4]

Species	Transition	Position [cm^{-1}]	Strength (296K) [cm^{-2}/atm]	min. Absorbance	Detectivity [ppm]
NO	$R_{2e}(7.5)+R_{2f}(7.5)$ $R_{1e}(7.5)+R_{1f}(7.5)$	5568.23 5568.30	6.81×10^{-4} 1.27×10^{-3}	4.24×10^{-4}	20
N_2O	P(14)	6567.29	5.72×10^{-4}	4.50×10^{-5}	6
CO	R(13)	6393.18	3.26×10^{-4}	4.50×10^{-5}	9
CO_2	R(16)	6359.97	4.22×10^{-4}	4.50×10^{-5}	7

Table 2 Transitions, line positions, and line strengths used for the sampling experiments. The calculated detectivities are based on the measured minimum absorbances in a 20-Hz bandwidth and a 1-sec measurement time.

Figure 11 shows a single-sweep measurement of the CO R(13) line (296 K, 214 torr, 230 ppm CO). The residual represents the normalized difference between the best-fit Voigt profile and the data. The minimum measured detectableabsorbance was 4.5×10^{-5} (20-Hz noise bandwidth, 1-sec measurement time) and corresponded to a CO detectivity of 9 ppm.

Table 2 lists the transitions, line positions and strengths that were used for the sampling experiments. The calculated species detectivities of the diode-laser sensor system are based on the measured minimum detectable absorbance for a 20-Hz noise bandwidth and a 1-sec measurement time. Measurements of NO were limited by étaloning from the fiber couplers and from (Ge) detector noise. Properly coated optical components could enhance the detectivity of NO to 2 ppm (calculation based on min. detectable absorbance of 4.5×10^{-5} in a 20-Hz noise bandwidth and 1-sec measurement time). Measurements of N_2O, CO, and CO_2 were limited by interference effects in the absorption cell, optical components, and laser cavity.

3.2 Sampling Experiments

As the first set of sampling experiments, calibrated flows of 30% NH_3/N_2 (NH_3 injection of 0.13 l/min and 0.07 l/min) were added to the premixed gases of CH_4 and air. NO mole fractions in the post flame region of the premixed, laminar, flat flame were determined from measured absorption of probe-sampled combustion gases in the multipass cell. Measured NO mole fractions of the dried samples were converted to wet-basis mole fractions by assuming that water vapor equal to the equilibrium value at the metered equivalence ratio and measured temperature had been removed.

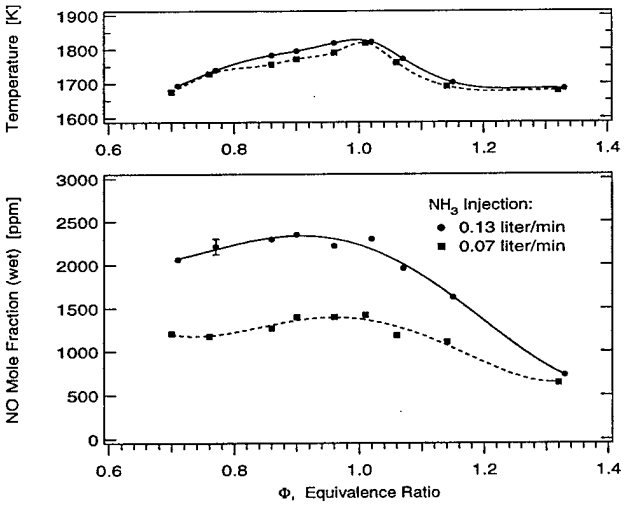

Fig. 12 Measured temperatures and NO molefractions (wet basis) as a function of equivalence ratio and injected NH_3 flow rate in a premixed, NH_3 seeded CH_4/air flame.

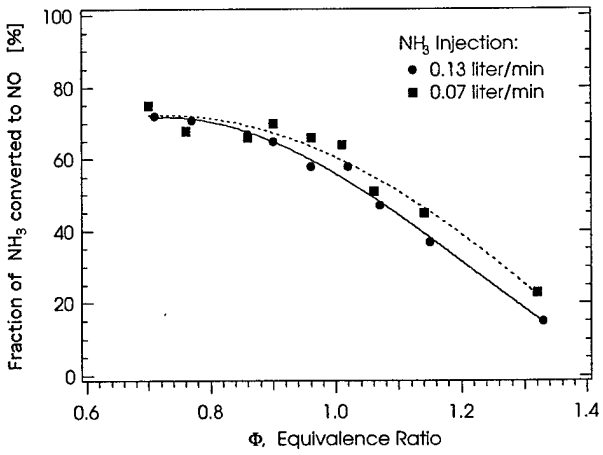

Fig. 13 Fraction of NH_3 converted to NO as a function of equivalence ratio and injected NH_3 flow rates.

Figure 12 shows the measured temperatures and NO concentrations (wet basis) as a function of equivalence ratio and injected NH_3 flow rate. Temperature measurements were on average 15 K higher for the higher NH_3 flow rate. The measured NO molefractions increased for both injected NH_3 flow rates with equivalence ratio from Φ=0.7 to 1.0 by ~11% (0.13 l/min NH_3 injection) and ~19% (0.07 l/min NH_3 injection). For fuel rich conditions, the measured NO molefractions decreased with increasing equivalence ratio (Φ=1.02 to 1.33) by ~68% (0.13 l/min NH_3 injection) and ~54% (0.07 l/min NH_3 injection).

Figure 13 provides a plot of converted NH_3 to NO as a function of equivalence ratio and injected NH_3 flow rate. For fuel-lean conditions, the measured average fractions of NO converted to NH_3 (68%) compared well with previously published results (70%).[15] For fuel rich conditions, the average NH_3 to NO conversion decreases from 68% to approximately 20% at Φ=1.33. The NH_3 conversion is ~35% higher for the lower NH_3 injection rate (0.07 l/min) compared to the higher NH_3 injection rate (0.13 l/min) at Φ=1.3.

A second set of sampling experiments were performed to measure CO and CO_2 concentrations in the post-flame gases above a premixed CH_4/air flame. Species mole fractions were calculated from measured absorption in probe-sampled combustion gases, measured cell pressure and temperature, and known line strengths. The measured CO and CO_2 molefractions (dry basis) are shown as a function of equivalence ratio in Figure 14. The solid lines represent chemical-equilibrium calculations of the respective species mole fractions at measured temperatures (top half of Figure 14). The vertical bars represent the uncertainty in measured species mole fractions due to line strength and measurement uncertainty.

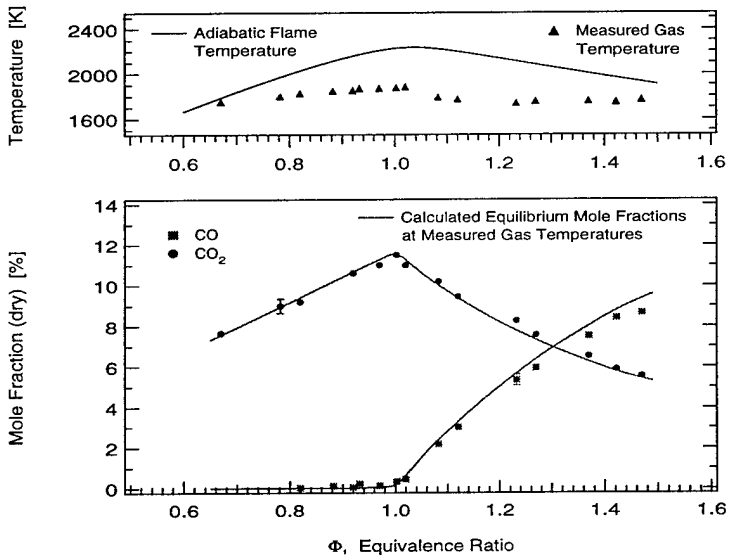

Fig. 14 Comparison of measured CO and CO_2 mole fractions (dry basis) to calculated equilibrium values at measured temperatures.

The CO_2 data agree to within 3% with calculated equilibrium values in the fuel-lean region. For Φ>1 the measured CO_2 mole fractions are slightly higher and the measured CO mole fractions are slightly lower than the calculated equilibrium values, suggesting a partial conversion of CO to CO_2 in the sampling probe. The partial conversion is likely due to surface kinetics effects and the finite residence time in the probe.[4] NO and N_2O were not detected in the post-flame gases, indicating that concentrations were below the respective detection limits.

4. CONCLUSIONS

A fiber-optic diode-laser absorption sensor system has been developed to measure NO, N_2O, CO, CO_2 concentrations using absorption spectroscopy and fast-extraction probe sampling techniques. The system was applied to measure NO mole fractions in the post-flame gases of a premixed CH_4/air flame seeded with NH_3. In addition, CO and CO_2 molefractions were measured in the combustion products of a non-seeded, premixed CH_4/air flame.

Measured room-temperature survey spectra of NO in the spectral region from 5556–5572 cm^{-1} (~1.8 μm) compared favorably with calculated values. In addition, measurements of H_2O survey spectra were recorded in this spectral region to select optimum NO lines with maximum detectivity and minimum H_2O interference for NO concentration measurements. Measured survey spectra of the N_2O $3\nu_3$ band (6535–6600 cm^{-1}) were used to select appropriate transitions for N_2O measurements.

Sampling experiments with a CH_4/air flame seeded with NH_3 showed that for fuel-lean conditions approximately 70% of the injected NH_3 was converted to NO. For fuel-rich conditions, the fraction of NH_3 converted to NO decreased from 68% ($\Phi \leq 1$) to approximately 20% (Φ=1.33). In sampling experiments in a non-seeded, premixed CH_4/air flame, measured CO concentrations were slightly lower and measured CO_2 concentration were slightly higher than calculated equilibrium values for fuel-rich conditions indicating partial conversion of CO to CO_2 in the sampling probe. This system may be applied for continuous measurements of NO, N_2O, CO and CO_2 in stack gases of combustion systems for open- and closed-loop applications.

ACKNOWLEDGMENTS

The authors thank R. J. Gessman and C. O. Laux (Stanford University) for providing the calculations of NO line positions and strengths for the 3ν band and Anritsu Corporation, Japan for the 1796-nm DFB diode laser.

This research was supported by the Strategic Environmental Research and Development Program, with K. Schadow as technical monitor, and by the U. S. Air Force Office of Scientific Research, Directorate of Aerospace and Materials Sciences, with J. Tishkoff as technical monitor.

REFERENCES

1. D. M. Sonnenfroh, M. G. Allen, and W. J. Kessler, "The evolution of a room temperature, near-IR diode laser sensor for combustion generated NO emissions," paper AIAA 97-0321 at the 35th AIAA Aerospace Sciences Meeting, Reno, NV, January 6–10, (1997).
2. E. R. Furlong, D. S. Baer, and R. K. Hanson, "Combustion control using a multiplexed diode laser sensor system," Twenty-Sixth Symposium (International) on Combustion, 2851–2858, The Combustion Institute, Pittsburgh, (1996).
3. M. F. Miller, W. J. Kessler, and M. G. Allen, "Diode laser-Based Air Mass Flux Sensor for subsonic aeropropulsion inlets," Appl. Opt. **35**, 4905–4912 (1996).
4. R. M. Mihalcea, D. S. Baer, and R. K. Hanson, "Diode-laser sensor for measurements of CO, CO_2, and CH_4 in combustion flows," Appl. Opt. (in print) (1997).
5. Shang-I Chou, D. S. Baer, and R. K. Hanson, " Diode laser absorption measurements of CH_3Cl and CH_4 near 1.65 μm," Appl. Opt. **36**, 3288–3293 (1997).
6. R. M. Mihalcea, D. S. Baer, and R. K. Hanson, "Tunable diode-laser absorption measurements of NO_2 near 670 and 395 nm," Appl. Opt. **35**, 4059–4064 (1996).
7. D. S. Baer, R. K. Hanson, M. E. Newfield, and N. K. L. M. Gopaul, "Multiplexed diode-laser sensor system for simultaneous H_2O, O_2, and temperature measurements," Opt. Lett. **19**, 1900–1902 (1994).
8. C. T. Bowman, "Control of combustion-generated nitrogen oxide emissions: technology driven by regulation," Twenty-Fourth Symposium (International) on Combustion, p. 859, The Combustion Institute, 1992.
9. G. Herzberg, "Spectra of diatomic molecules," in *Molecular Spectra and Molecular Structure* (Krieger Publishing Company, Florida, 1989), Vol. 1, pp. 268–270.
10. C. Amiot, "The infrared emission spectrum of NO: analysis of the Δv=3 sequence up to v=22," J. Molec. Spec. **94**, 150–172 (1982).
11. S. R. Langhoff, C. W. Bauschlicher Jr., and H. Prtridge, "Theoretical dipole moment for the $X^2\Pi$ state of NO," Chem. Phys. Lett. **223**, 416–422 (1994).

12. M. N. Spencer, C. Chackerian, Jr., and L. P. Giver, "The nitric oxide fundamental band: frequency and shape parameters for rovibrational lines," J. Molec. Spec. **165**, 506–524 (1994).
13. V. Dana, et al., "Λ-Splittings and line intensities in the 2←1 hot band of nitric oxide," J. Mol. Spectrosc., **165**, 525–540 (1994).
14. A. Campargue, et al., "Overtone spectroscopy in nitrous oxide," J. Chem. Phys. **103**, 5931–5938 (1995).
15. R. J. Martin and N. J. Brown, "Nitrous oxide formation and destruction in lean, premixed combustion," Combust. Flame **80**, 238–255 (1990).